

Correlation of photocurrent and electroabsorption spectra and their temperature dependence for conjugated light emitting polymers: The origin of the corresponding density of states

Awnish K. Tripathi^{1,2} and Y. N. Mohapatra^{1,2,3,*}¹*Department of Physics, Indian Institute of Technology Kanpur, Kanpur 208 016, India*²*Samtel Center for Display Technologies, Indian Institute of Technology Kanpur, Kanpur 208 016, India*³*Materials Science Programme, Indian Institute of Technology Kanpur, Kanpur 208 016, India*

(Received 9 July 2011; revised manuscript received 22 October 2011; published 18 November 2011)

Photocurrent (PC) and electroabsorption (EA) spectra of two different families of light emitting conjugated polymers viz. poly[2-methoxy-5-(2'-ethylhexyloxy)-1,4-phenylenevinylene] (MEH-PPV) and Arylenevinylene-co-pyrrolinevinylene (C8-AVPV) in standard sandwich diode configuration is measured. It is shown that EA spectra with a dominant positive peak at the onset has identical line shape as that of the first derivative of the PC spectra for both the materials. The temperature dependence of onset EA peak is studied in detail in the temperature range 10–300 K, and show redshift and narrowing with decrease in temperature. The temperature dependence of the signal height in the case of PC follows that of carrier mobility, while EA peak height follows occupancy within the density of states (DOS). At room temperature, the EA peak height shows very slow and nonexponential transients indicating relaxation in occupancy of states. The degree of nonexponentiality is seen to decrease with increase in reverse bias. The set of observations lead to the conclusion that the onset positive peak in both types of spectra is dominated by photoionization of localized states whose occupancy depends on the Fermi level, which in turn is controlled by variation in bias and temperature. A phenomenological model illustrating the origin of equivalence between EA and PC onset features is described. It is argued that the occurrence of a positive peak at the onset in such spectra, obtained for diode structures, is a signature of photoionization of defect states and the line shape corresponds to its polaronic DOS; hence correlation of PC and EA becomes a direct and powerful method of determination of near-gap joint DOS in molecular semiconductors.

DOI: [10.1103/PhysRevB.84.205213](https://doi.org/10.1103/PhysRevB.84.205213)

PACS number(s): 81.05.Fb, 73.50.Pz, 71.23.-k, 78.40.Me

I. INTRODUCTION

The molecular semiconductor based technologies for large area electronic applications and flexible displays are crucially dependent on a detailed understanding of their photoelectronic properties in thin-film form in which they are typically used in devices.¹ The possible commercial applications, such as large area displays, photovoltaic cells, sensors, and lighting, are being demonstrated routinely with improved performances.² A correlation between optical properties and carrier transport is central to the understanding of fundamental physics issues and their applications as photoelectronic materials. About a decade ago, this had given rise to a fierce debate regarding the nature of fundamental excitation, which is the crucial link between absorption of photon and eventual carrier generation and their transport. Many of the issues of the earlier debate on applicability of models linger on to date in some form or the other.³

The variation of extent of localization from molecule to solid-state thin film on the one hand and role of defect and disorder in energetics on the other lends itself to the possibility of multiple views in the interpretation of observed properties. In these electronic systems, most of the optoelectronic processes and properties have been described using the framework of Gaussian density of states (DOS), the origin of which have been attributed to the disorder in thin-film form.⁴ Being amorphous in nature and having little or no free charge carriers available for conduction, these materials are essentially insulators; however, their semiconducting aspect is achieved through electrical or optical means of charge-carrier injection.

Among the experimental studies employed, the techniques of photoconductivity and electroabsorption spectra played a

central role. Photoconductivity as a phenomenon is significant in the study of the interplay between generation of free carriers due to photon absorption and its subsequent conduction.^{5,6} Interpretation of the photogeneration process in these disordered molecular solids has guided research on solar cells and sensors.^{1,2,5,7} Photocurrent (PC) action spectrum measurement both in the steady-state and transient situations, and its temperature and electric field dependence, have been used to study the photogeneration mechanism,^{5,6,8,9} effect of trapping,¹⁰ and exciton diffusion dynamics^{11,12} in organic thin films. Specifically, for example, the observed correlation of photocurrent (PC) onset and absorption threshold in conjugated polymers, viz. poly(p-phenylene vinylene) (PPV) and its soluble derivatives, have been argued to favor a traditional band model,^{5,6} while the observed lack of such correlation in polydiacetylenes was taken to be the evidence of the molecular exciton model.^{3,5}

Furthermore, the absorption together with electroabsorption (EA) spectrum has also been used to investigate photoexcitation processes in conjugated polymers,^{13–15} where a derivative-like feature is observed in EA at the low-energy onset of absorption and has been assigned to transitions in excitonic levels. A detailed study of dilute blends of poly[2-methoxy-5-(2'-ethylhexyloxy)-1,4-phenylenevinylene] (MEH-PPV) thin films have been carried out by Hagler, Pakbaz, and Heeger,¹³ where EA spectra were fitted using the continuum version of the Su-Schrieffer-Heeger (SSH) model.¹⁶ The EA spectral line shape at low energy was assigned to intrinsic property of an ordered π -electronic system of oriented MEH-PPV. Later, Liess *et al.*¹⁴ argued that the presence of conjugation length distribution and phonon coupling (ignored in the Hagler model¹³) show essential

influence on the EA line shape. Also, disordered polymer films exhibit noticeable inhomogeneous broadening of the first derivative of absorption deviating from the EA line shape. They proposed a sum over three essential excitonic states (SOS) model (ground state $1A_g$, lowest odd-parity excited state $1B_u$, and even-parity excited state mA_g strongly coupled to $1B_u$), in which their phonon replicas and an asymmetric Gaussian distribution of conjugation lengths was considered (having eight free fitting parameters). Martin *et al.*¹⁵ remarked that, in SOS model,¹⁴ an odd-parity three photon state nB_u must be included in the calculation, the presence of which has been supported by a third harmonic generation measurement by Mathy *et al.*¹⁷ Also, they argued that the response of the nB_u state is masked due to inclusion of vibrational coupling in Liess's calculation. They fitted the EA spectrum of both PPV and MEH-PPV using a four-essential-state ($1A_g$, $1B_u$, mA_g , and nB_u) model and for a distribution of conjugation length. The level of complexity of the models has prevented its widespread use to extract parameters of significance, such as the degree of disorder.

Most of the applications are crucially dependent on transport properties, which in turn are controlled by the nature of disorder and defects and their eventual expression as electronic density of states. Though a general understanding of transport in the presence of disorder has emerged through the framework of the Gaussian density of states and its many variants, information specific to electronic quality of materials and devices in terms of electrical origin of defects and their influence is still lacking. The onset feature in EA and PC is known to carry information of density of states around the energy of the highest occupied molecular orbital (HOMO) - lowest unoccupied molecular orbital (LUMO) gap. Hence a careful study of the onset feature can be helpful to determine the electronic quality of organic thin films in practice.

To state our motivation clearly in this context, we would like to point out several major shortcomings of the studies so far in the literature as listed below.

(i) Most of the results of early EA studies have been carried out using a planar geometry with interdigitated electrodes,^{13–15} while present-day samples being thin films sandwiched between electrodes are more appropriate for practical applications.^{18–22} The differences in EA spectra between planar and sandwiched geometry have been noted in the literature.^{19,20} In such sandwiched samples, there is a positive peak in EA at the onset that dominates over the negative part.^{19–22} This is attributed to either the choice of the electrodes¹⁸ or as an experimental artifact¹⁹ due to strong absorption in reflection geometry. Hence contribution from possible intrinsic reasons to this difference can get masked. In addition, the degree of control in the quality of thin films and devices has improved over the years significantly.

(ii) Rarely have the same samples (or those prepared under similar controlled conditions) been subjected to detailed EA and PC studies simultaneously enabling comparison of the onset feature in these two important techniques.

(iii) The temperature dependence of the onset feature in EA and PC has not been systematically studied except for noting spectra either at room temperature or at 77 K.^{13,14}

In this paper, we focus on the systematic correlation of the low energy onset features in PC and EA of two otherwise well-characterized polymer thin films in sandwiched

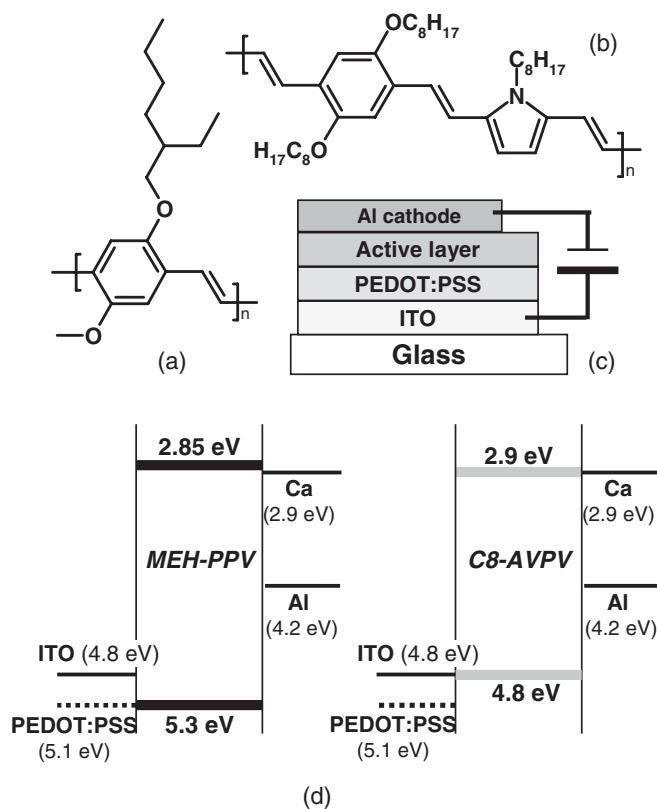


FIG. 1. Molecular structure of active material (a) MEH-PPV, (b) C8-AVPV, (c) device configuration, and (d) band diagrams for MEH-PPV and C8-AVPV sandwiched devices.

geometry typical of real applications. The attempt here is to recover empirically significant parameters, such as the peak-energy and broadening parameter, which can then be confronted with well-formulated theory and be used for electronic quality assessment. We systematically follow the temperature dependence of these parameters to disentangle absorption and transport properties. The observed behavior of the lowest energy onset features points to the involvement of relevant density of states and their occupation in the excitonic processes.

For the study, we choose two different families of conjugated light emitting polymers, viz. poly[2-methoxy-5-(2'-ethylhexyloxy)-1,4-phenylenevinylene] (MEH-PPV) and Arylenevinylene-co-pyrrolenevinylene (C8-AVPV) in a typical sandwiched device configuration. Here MEH-PPV is an extensively studied material, while C8-AVPV has been synthesized in our lab and otherwise characterized extensively.²³ The chemical structures of both the polymers are depicted in Figs. 1(a) and 1(b). Their sandwiched device configuration and band diagrams are schematized in Figs. 1(c) and 1(d), respectively. The HOMO and LUMO values for the C8-AVPV polymer have been obtained using conventional cyclic voltammetric technique and photoluminescence measurements.²³ The band diagrams shown here are for two different cathodes, calcium (Ca) and aluminum (Al); however, for the purpose of the present study, a thick Al cathode is preferred. We also note that EA measurements have already been reported in sandwiched devices of conjugated polymers, though in an entirely different context.^{18–22} These two polymeric systems,

despite having different backbone and being classified under two different families, are however helpful for establishing a general notion of DOS in such electronic systems.

We deliberately take an empirical route of enquiry instead of fitting to any preexisting models and keep data and our interpretation separate as far as possible. We demonstrate the relation of first derivative of the flux normalized PC action spectrum with that of EA spectrum for both the polymers. In order to isolate various cross-sensitive parameters, we carry out a temperature-dependent (10–300 K) study of EA spectra, and discuss the nature of the DOS through voltage dependent transient EA (t-EA) measurements.

II. EXPERIMENTAL METHODS

All the devices are fabricated in controlled laboratory conditions as much as possible to avoid any extrinsic effect on the optoelectronic properties of the material studied. Commercial indium tin oxide (ITO) coated glass substrates are used, which serve as a transparent electrode. The patterned and RCA cleaned ITO substrates are subjected to a 15-min ozone treatment, followed by spin-coating of a thin layer of poly(3,4-ethylenedioxythiophene):poly(styrene sulfonate) (PEDOT:PSS), and baked at 120 °C for 1 h under 10^{-7} mbar vacuum. The PEDOT:PSS layer serves as a buffer layer to avoid the high electric field associated with roughness of the ITO substrates. The solution of MEH-PPV (obtained from commercial source Sigma Aldrich) is prepared with concentration of 6 mg/cc in chloroform:toluene (50:50) mixture, which was optimized from the point of view of device fabrication in our laboratory.²⁴ C8-AVPV polymer solution is prepared in chlorobenzene with a concentration of 10 mg/cc. Active layers are spin-coated and dried under 10^{-7} mbar vacuum at 120 °C for 1 h. The Al cathode, functioning as a reflective electrode, is deposited through shadow mask without breaking the vacuum to avoid any contamination at the active layer-cathode interface. The device structure [Fig. 1(c)] thus obtained is ITO/PEDOT:PSS/active layer/Al with active layer thickness of ~ 100 nm, measured using profilometer (Tencor alpha-step 500).

The schematic diagram of the experimental setup for the combined PC and EA measurement is shown in Fig. 2. Both PC and EA measurements are performed employing a standard

lock-in technique to achieve a high signal-to-noise ratio. All the measurements are done in a cryostat capable of going down to 10 K. The temperature of the device is monitored using a Si diode mounted on a specially designed sample holder for low-temperature measurements. The monochromatic light, derived from a white light source (Tungsten-Halogen lamp, QTH) is focused through ITO layer, normal to the device area in the case of PC and at an angle of 45° in the case of EA. The PC is monitored under zero bias condition across the devices and hence any transport of charge carrier involved in PC is only due to built-in voltage ($V_{BI} \approx 0.6$ V) of the device. The EA measurements are preferred here in the reflection geometry scheme as Al serves as a better reflecting electrode. Also, significant EA signal can be achieved using low bias voltages (typically of the order of few volts), which are also safe for a sandwiched structure avoiding device breakdown. In contrast, a coplanar geometry scheme, which is far from realistic applications,^{13–15} requires biases of the order of kV for significant EA signal.

In the presence of a dc electric field (if $V_0 \neq 0$), the EA response is modulated both at the fundamental and the second harmonic frequency of the applied ac bias.¹⁸ The EA response at the fundamental frequency is given as

$$-\frac{\Delta R}{R}(h\nu, \omega) \propto \text{Im}(\chi^{(3)})(h\nu)V_0V_{ac} \sin(\omega t), \quad (1)$$

where $\chi^{(3)}$ is the third-order nonlinear susceptibility, $V_0 = V_{dc} - V_{BI}$ is the total static voltage across the device, V_{BI} is the built-in voltage, V_{ac} is the applied ac bias, and ω is the frequency of the applied ac bias. The contribution to $\chi^{(3)}$ can come from a variety of sources, viz. presence of permanent dipole moments, polarizability difference between ground and excited states or mixing of electronic states, and polarization due to localized states. Any field-induced absorption mechanism would therefore influence the line shape measured in such experiments. The dc and ac bias for EA measurement are -5 and 1 V respectively. The EA in the reverse bias situation ensures appearance of uniform electric field across the device, in the absence of charge carrier injection and transport. The possibility of accumulation of charges at any interface is insignificant in this case. Also, modulated electroluminescence (EL) at the reference modulation frequency of V_{ac} is expected in the forward bias case, which could influence the observed

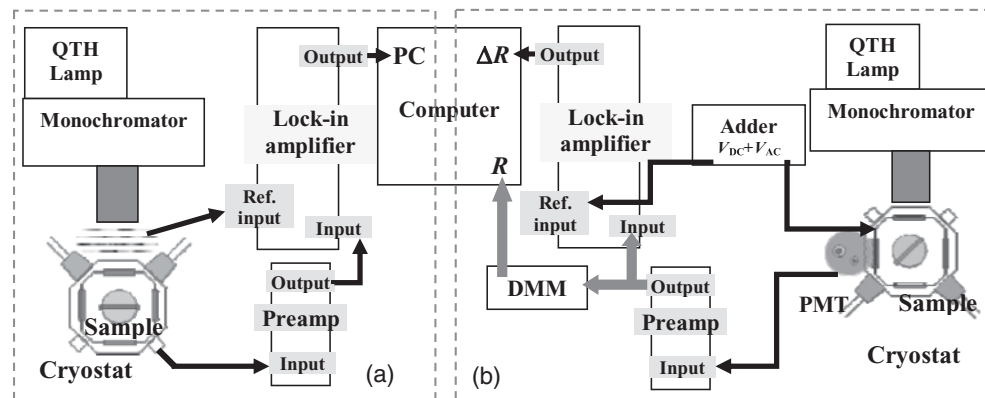


FIG. 2. Low temperature setup for (a) PC action spectrum measurement and (b) EA measurement.

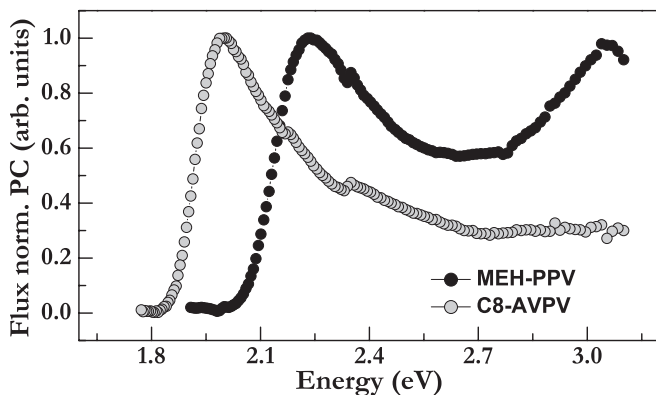


FIG. 3. Photon flux normalized PC action spectra for MEH-PPV (black filled circle), and C8-AVPV (gray filled circle), for ITO/PEDOT:PSS/active layer/Al configuration. The feature at 2.3 eV is known to be due to an experimental artifact in our experiments while carrying out flux normalization procedure.

EA signal. The optimum EA signals are obtained for a low modulation frequency of $\omega = 33$ Hz, which was also used as a reference frequency for PC measurements.

III. RESULTS AND DISCUSSION

A. Room temperature PC action spectra and EA spectra

Figure 3 shows photon flux normalized PC action spectra for MEH-PPV and C8-AVPV thin films under zero bias at room temperature. To normalize the as-measured PC action spectrum with respect to intensity of the excitation source, the spectral response of the measurement system was recorded under identical conditions using a flat response PMT. For MEH-PPV, it matches well with reports in the literature,⁶ while that of in-house developed C8-AVPV is being reported here for the first time, though other extensive photoelectronic properties have been reported elsewhere.²³ The differences observed between the two polymers can be attributed to the difference in structure of the backbone. The feature observed at ~ 2.3 eV has been confirmed to be due to an artifact of flux normalization procedure, which is present in both cases.

The EA spectra for MEH-PPV and C8-AVPV are shown in Fig. 4 in the same device configuration as used in PC. Note the asymmetry observed in positive and negative wings of EA spectra for both cases, the origin of which was a source of debate in both types of devices with interdigitated electrodes^{13–15} and in sandwich structure.^{18,19,21} The line shape in reflection geometry measuring $\Delta R/R$ is often considered equivalent to $\Delta T/T$ in transmission mode, in the absence of electroreflectance.^{19,20} For a strongly absorbing case, the spectrum can get modified in reflection mode as shown in Appendix A. However, the positive peak of EA does not get affected since it occurs in the low absorption region as demonstrated in the same Appendix. Giebler *et al.*¹⁹ have reported this difference in the line shape between planar and sandwiched samples as an experimental artifact. For the purposes of the present work, it suffices to note that the EA positive wing line shape of MEH-PPV matches well with

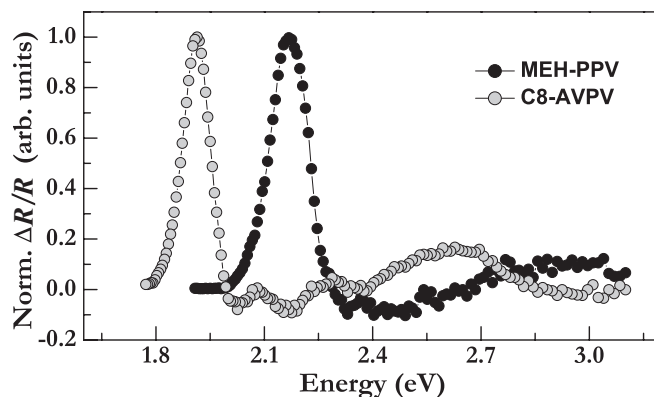


FIG. 4. Electroabsorption spectra for MEH-PPV (black filled circle), and C8-AVPV (gray filled circle), in ITO/PEDOT:PSS/active layer/Al configuration.

other reports.^{13–15,18–22} The symmetric feature at the onset observed in the EA spectra for these polymeric systems has been attributed to $1B_u$ excitonic level in literature.¹⁴

B. EA and PC-derivative line shape comparison

Figure 5 shows a comparison and very good match between the EA line shape with first derivative of PC for the low-energy part of the spectra at room temperature, for both MEH-PPV and C8-AVPV. This striking fact directly points to the common origin of the two phenomena, and that the energy states involved in the positive peak in the two cases must be identical. The onset of photoconductivity can be considered as a combined process involving photon absorption, formation of excitons, dissociation of excitons creating charged carriers, and their transport to respective electrodes. In contrast, EA only involves absorption due to those differential energy states that experience the field modulation. The coincidence of the first derivative of PC with the EA spectrum at the onset therefore means that the line shape corresponds to the shape of DOS. We provide an explanation in our later discussion and

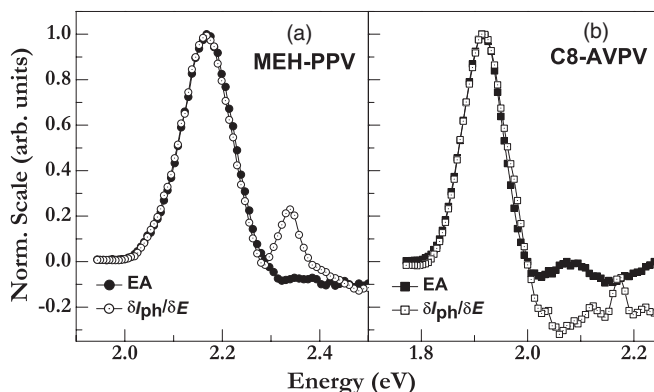


FIG. 5. Plot comparing the positive line shape of EA and first derivative of PC action spectra for (a) MEH-PPV and (b) C8-AVPV. Note that the peak at ~ 2.3 eV in PC derivative spectrum for MEH-PPV cases is an artifact in the experimental setup as pointed out in the previous section.

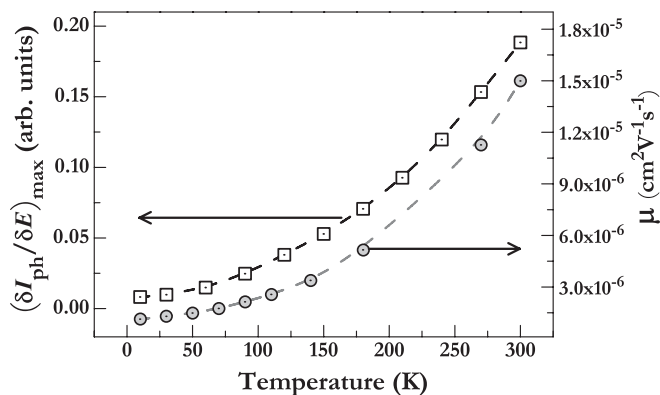


FIG. 6. Temperature dependence of magnitude of PC derivative at the peak and mobility (measured by transient electroluminescence method²⁵).

illustrate the relationship between the EA and PC spectra in Appendix B at the end.

C. Temperature dependence of EA and PC

Figure 6 shows the temperature dependence of the magnitude of PC derivative peak and compares it with the observed temperature dependence of mobility (measured by the transient electroluminescence method described in detail elsewhere²⁵) of the charge carrier. Clearly, the two are parallel to each other, showing that the temperature dependence of PC magnitude is controlled by transport. Though this conclusion is significant in itself, it also means that it is not possible to decouple DOS information from the signal strength of PC since both absorption and transport parameters determine its magnitude. The EA spectrum, on the other hand, does not involve transport of charge carriers and is only due to field-induced absorption with modulation of the energy state only near the transition energy, and hence would be proportional to the DOS. Therefore, we choose to concentrate on the spectral features further using temperature dependence of the EA line shape.

Figure 7 shows temperature-dependent EA spectra for MEH-PPV and C8-AVPV. It is easy to visualize systematic changes both in height and in spectral shape in such plots. We go on to describe in detail the significant features through parametrization using empirical fitting. At room temperature, maxima in the EA line shape appear at ~ 2.16 and ~ 1.92 eV for MEH-PPV and C8-AVPV, respectively. Though no change in onset energy is observed with decreasing temperature for both the polymers, there is a redshift of the line shape accompanied by peak narrowing. The negative dip in the EA spectrum following the peak maximum shifts toward lower-energy values with almost no change in the magnitude with decreasing temperature. There are noticeable systematics among other features in the data, but we will not dwell on them here. We will focus exclusively on the most significant features of the positive EA peak and analyze them at different temperatures.

For consistency of the fitting and reliable parameter extraction, several physically motivated functional forms were tried. As expected, the two most promising candidates turn out to be “asymmetric Gaussian” function $g(E)$ [Eq. (2)]

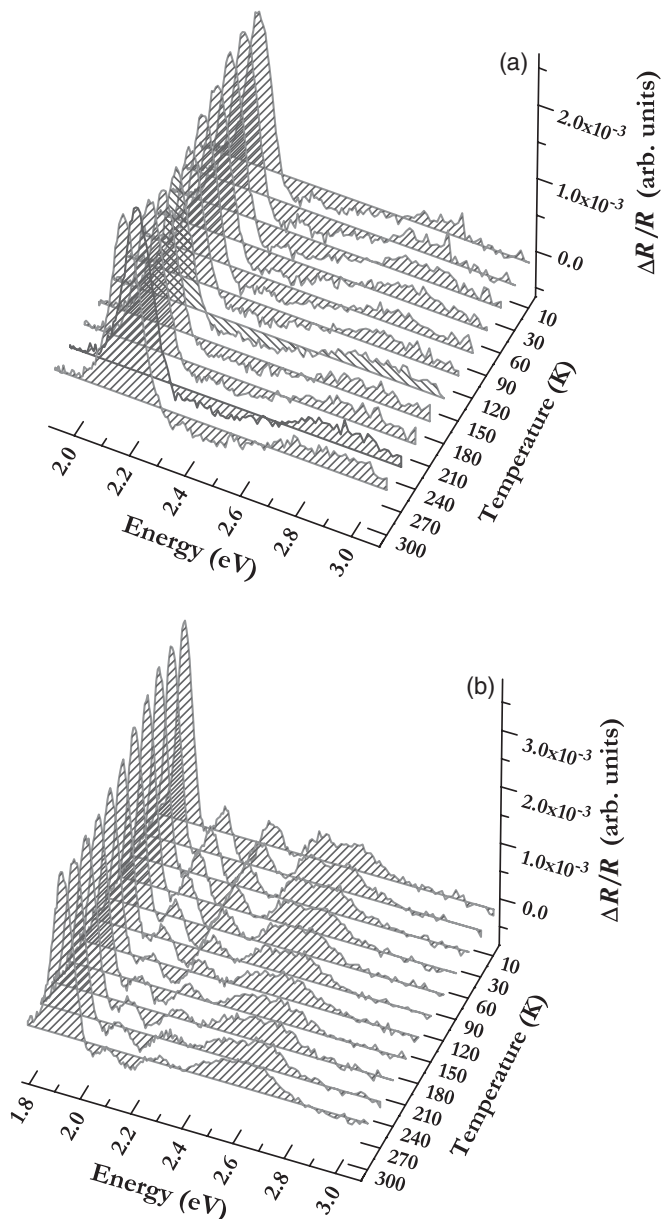


FIG. 7. Temperature dependent electroabsorption spectra for (a) MEH-PPV and (b) C8-AVPV.

and relation $h(E)$ [Eq. (4)], which is the “first derivative of a standard Gaussian” $g_1(E)$ as defined below:

$$g(E) = \frac{2A}{\sqrt{2\pi}(\sigma_1 + \sigma_2)} \begin{cases} e^{-\frac{1}{2}(\frac{E-E_c}{\sigma_1})^2}, & E < E_c \\ e^{-\frac{1}{2}(\frac{E-E_c}{\sigma_2})^2}, & E \geq E_c \end{cases} \quad (2)$$

and

$$g_1(E) = \frac{A_1}{\sqrt{2\pi}\sigma} e^{-\frac{1}{2}(\frac{E-E_c}{\sigma})^2}, \quad (3)$$

$$h(E) = g'_1(E) = -\{(E - E_c)/\sigma^2\}g_1(E), \quad (4)$$

where A is the area under the curve, E_c is the mean energy (location of the peak), and σ is the standard deviation of the Gaussian distribution.

The quality of fitting obtained using these two fittings is compared in Fig. 8 for three different temperatures for

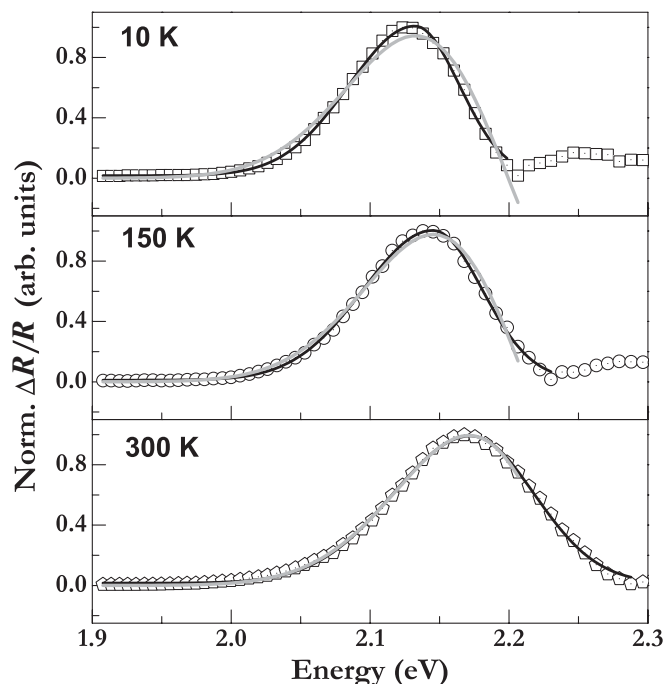


FIG. 8. Comparison between “derivative of Gaussian” model (gray line) and “asymmetric Gaussian” model (black line) at three different temperatures for MEH-PPV. Note that asymmetric Gaussian model fits well the positive wing of EA.

specificity. The derivative of Gaussian model exhibits a noticeable deviation at low temperature and only partially fits the EA spectrum. The asymmetric Gaussian, however, fits the spectrum reasonably well for the entire positive wing, and hence is selected for monitoring parameter variation as a function of temperature.

Figure 9 shows the details of analysis of the positive wing of EA for both polymers. The variation of peak energy and its width show parabolic dependence on temperature. This behavior provides a potential test for any successful theoretical or phenomenological model. We postpone this discussion and a possible explanation to a later section after presenting all other supporting empirical observations.

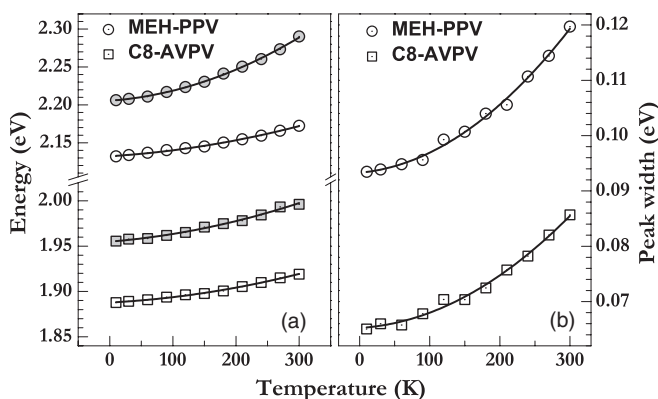


FIG. 9. (a) Temperature dependent shift of peak energy (unfilled) and zero crossing energy (gray filled) for MEH-PPV (circle) and C8-AVPV (square) and (b) corresponding peak width variation.

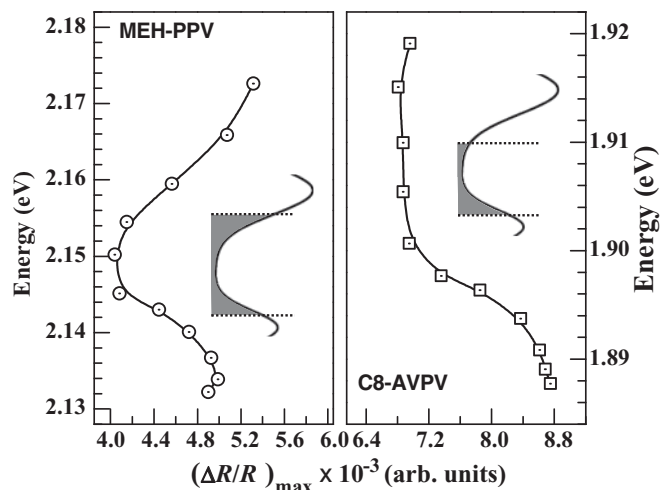


FIG. 10. Portion of the DOS being scanned as derived from temperature dependent EA magnitude at the peak $[(\Delta R/R)_{\max}]$ for MEH-PPV and C8-AVPV. The inset schematic shows the probable portion in a larger perspective for conceptual clarity.

The occupation statistics of the states involved in absorption can be traced by monitoring the maximum of EA onset peak $(\Delta R/R)_{\max}$ against the corresponding peak energy for different temperatures. Figure 10 shows such variation for both polymers in separate plots, where y axis is the peak energy and x axis is the corresponding peak height. The plots render the shape of the DOS over which the transition energy shifts with temperature. This is further illustrated with schematics of probable DOS with the region under observation shaded on the right side of the plots. A local minimum observed in each case is the indication that the portion under observation is the transition between two Gaussians.

D. EA transients

In order to trace the origin and nature of the density of states involved in the process, it is important to ascertain the time scale of changes in the occupation statistics. To do so we carry out voltage dependent electroabsorption transient measurements, i.e., we monitor $(\Delta R/R)_{\max}$ as a function of time in response to a step exposure sitting at the peak energy for different magnitudes of reverse bias. Figure 11 shows a typical set of such EA transients for different voltages.

The nonexponential nature of transients clearly indicates involvement of a continuously distributed DOS within the slice of energy accessible with field modulation. In such cases, it is expected that the functional form would be a stretched exponential with a mean time constant τ and a stretching factor β . The transients thus have been fitted to stretched exponentials as given in Eq. (5):

$$\Delta R/R(t) = (\Delta R/R)_{\max,\infty} + (\Delta R/R)_{\max,0} e^{-(t/\tau)^\beta} \quad (5)$$

These transients are fairly slow, yielding fitting parameters tabulated in Table I. The time constant shows a small variation with reverse bias, but more significantly the stretching factor β increases from 0.78 to 0.95, showing that the transients become more exponential with increase in reverse bias. The slow time scale and bias dependence are probably the strongest

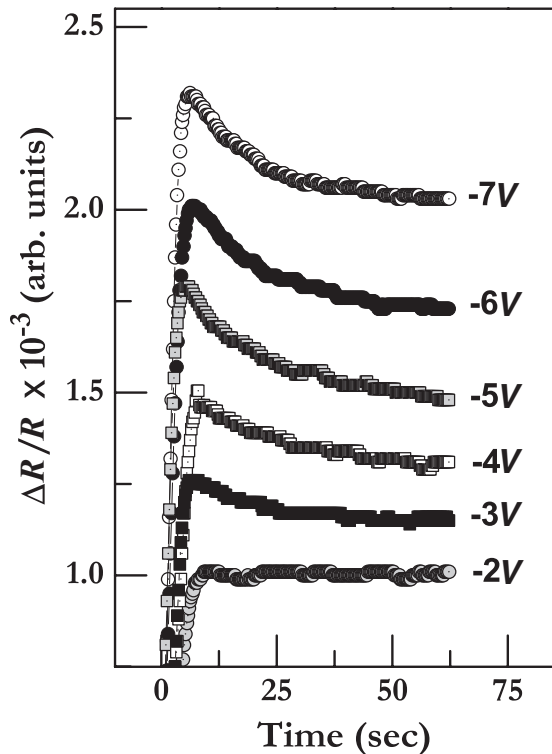


FIG. 11. EA peak signal transients at room temperature for different applied reverse bias, described by Eq. (5) and parameters in Table I.

evidence that most of the states involved corresponding to the onset peak are deep localized states in nature and not directly the excitonic states.

E. Putting it all together: the origin of DOS

Traditionally, the density of states in electroabsorption is considered to be due to excitonic states associated with the HOMO-LUMO gap and its distribution corresponding to distribution in conjugation length of molecular semiconductors.¹⁴ In the interpretation of PC, both excitonic states have been invoked to explain broadening of the onset,^{5,6} and sometimes photoionization of defects have also been referred to as a possible reason for onset broadening.^{5,26} We reiterate that our principal motivation behind a careful correlation between EA and PC for two different model polymers is to clarify the nature and origin of DOS involved so that they can be helpful in the study of the electronic quality of these materials in practice.

TABLE I. Extracted parameters from stretched exponential fitting of time resolved EA measurement at different reverse bias.

Voltage (V)	τ (sec)	β
-2	—	—
-3	17.99 ± 0.66	0.783 ± 0.027
-4	15.98 ± 0.35	0.802 ± 0.016
-5	15.98 ± 0.20	0.906 ± 0.012
-6	15.75 ± 0.23	0.940 ± 0.015
-7	12.95 ± 0.16	0.953 ± 0.012

On the basis of experimental facts presented so far in the foregoing sections, it is possible to develop a scenario consistent with the observed field variation and modulation, temperature dependence, and time dependence of EA spectra. The common origin of PC and EA is unmistakable from the agreement between EA and the first derivative of PC. We propose that the dominantly positive peak at the onset both in EA and first derivative PC spectra is principally due to photoionization of localized levels with much lesser contribution, if at all, from molecular excitonic states toward the higher energy side near the zero crossing. Recall that all our PC experiments are carried out at zero bias and hence the field is not sufficient for ionization of excitons. The source of field dependence need be explained if the low energy positive EA peak is to be attributed to photoionization. The modulation of the field as employed in the EA experiment is able to discretize the response from the states by varying the occupancy of the localized states near the Fermi level. Hence the correlation of evidence suggests that absorption at the onset is controlled by Fermi level movement of occupancy within the DOS. The relationship between DOS with PC and EA line shape is easily understood. We provide a simple and direct derivation in Appendix B of how, under the simple assumption of a constant photoionization cross section, the line shape in the spectra would be directly proportional to DOS in such a case.

In our view, the positive wing of the spectra is mainly due to the occurrence of photoionization and excitonic absorption with the former dominating in good diode-like sandwiched samples. The appearance of a well-formed negative wing^{14,19} (taking into account the corrections due to absorption) beyond the zero crossing is a guide to the contribution from the excitonic component. This view has important consequences for diagnostics. The EA line shape in sandwiched samples using reflection geometry therefore does not yield a distribution of conjugation length (often force-fitted to an asymmetric Gaussian distribution¹⁴), but it is the polaronic DOS of localized levels important from the point of view of transport and mobility determination. The need for invoking an asymmetric Gaussian while fitting can be due to two reasons. A combination of polaronic DOS and line shape of true excitonic EA transition would turn out to be of such a functional form. Even if the contribution from excitonic DOS is negligible, the product of Gaussian DOS and occupancy function dictated by Fermi level would lead to such an asymmetry.

The transitions from localized to band states have earlier been invoked to explain the broadness in EA line shape and absorption while attributing the fundamental absorption to single-particle band structure.^{5,13} If the excitonic absorption is considered as fundamental,¹⁴ all of the broadness is then attributed to distribution of conjugation length without providing a cogent explanation for occurrence for asymmetry of distribution. Our results show that occurrence of absorption due to defects can be dominantly attributed to the positive peak, irrespective of the mechanism for absorption at higher energy including that of excitonic origin.

The spatial location within the sample from which one obtains the spectral signal is also easy to visualize. This is illustrated with the help of the schematic energy band diagrams in Fig. 12, where we show that the region of crossing between the defect energy level within the HOMO-LUMO gap and the

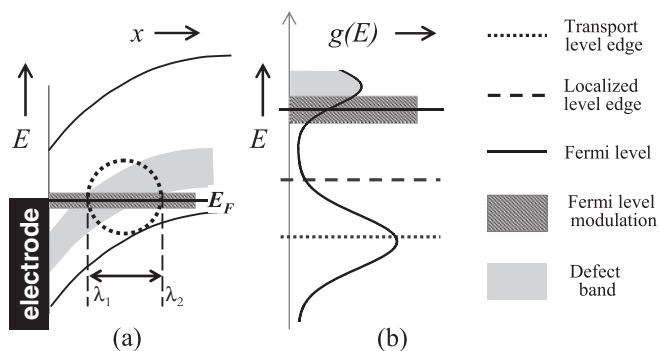


FIG. 12. Schematic of Fermi level crossing with a defect band resulting in (a) a transition region $\lambda_1 - \lambda_2$, whose occupancy gets modulated with modulation of E_F ; (b) corresponding DOS occupation for a “hole” band above HOMO band. The band bending due to defect charge is shown relative to the Fermi level, as is familiar in reverse biased Schottky diodes for simplicity.

Fermi level E_F determines the region of transition between filled and unfilled states. PC would be sensitive to all states below the Fermi level, since the absorption of a photon would create a hole by promoting the electron to the LUMO. In the case of EA, the response would be from the states near the crossing point experiencing field modulation and hence variation in occupancy.

The variation of spectra with temperature, such as change in peak energy (Fig. 9), and corresponding change in height (Fig. 10) can also be understood in terms of Fermi level movement within the DOS. As temperature is lowered, E_F moves toward the middle of the HOMO-LUMO gap, and hence a new slice of DOS participates, making the spectral height proportional to the corresponding DOS. The local band bending around the Fermi level would be approximately parabolic for a constant charge density in the vicinity. The shift of the crossing point of E_F with band bending would then explain the observed trends. The temperature dependence of peak energy shifts in luminescence experiments is typically attributed to change in the distribution of conjugation length along with assumptions regarding the Huang-Rhys coupling constant.²⁷ Such an explanation though is appropriate only if one is sure that one is dealing with a truly excitonic mechanism.

The observation of slow transients, as discussed earlier, is clearly due to slow change in defect occupancy with change in E_F through bias. We have already shown that the transients are less nonexponential at higher bias indicating the involvement of smaller distribution in energy. We seek to qualitatively explain this using the schematic in Fig. 13. The change in the degree of nonexponentiality can now be explained on the basis of the energy spread within the transition region of E_F crossing with the localized DOS. As the reverse bias is increased, the spread in energy within the transition region decreases due to higher band bending, which in turn leads to higher misalignment between the localized densities of states within the region. Hence a smaller slice defect DOS contributes to the transient at higher bias.

With this view, the asymmetric EA or derivative PC line shape becomes a powerful technique for obtaining polaronic DOS in typical sandwich diode structures. In early studies

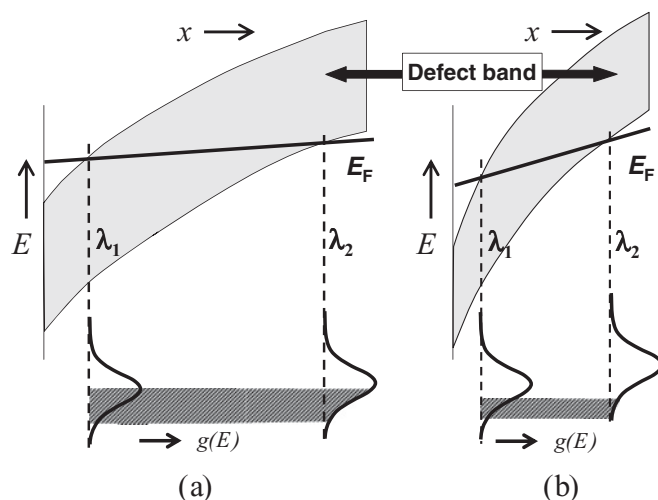


FIG. 13. Blown-up schematic of the crossing between Fermi level (as shown in Fig. 12) and defect band for two different reverse bias conditions. For low bias (a), the width of occupied energies is larger than the higher bias case (b). The DOS is shown only at the edges of the transition region. The defect levels are assumed to follow the band bending due to additional charges as in the case of reverse biased diodes.

employing surface interdigitated electrodes, this was not possible, since the typical separation between electrodes would be several microns and any signal due to the transition region would be negligible. Further, one can also understand the electrode dependence of asymmetry^{18,21} in terms of possible pinning of the Fermi level depending on the choice of electrodes and the concentration of defects at the transition points.

The DOS of conjugated polymeric systems is typically obtained from numerical simulation and parameter fitting.^{4,28–30} Reports of experimental DOS determination so far have been centered on measurement of mobility of carriers under a variety of experimental conditions.^{4,28–32} In these measurements, typically DOS and mobility (μ) products have been monitored. However, dependence of mobility on site energy distribution, electric field (F), and temperature (T) requires complicated deconvolution to obtain true energy dependence, rarely possible in practice. The dependence of concentration of doping on mobility has been used also to deduce DOS in LED and FET structures.³² DOS have also been estimated for specially designed samples employing expensive and relatively cumbersome procedures.^{33–35} The disorder parameter σ thus deduced clearly lacks the directness and spectroscopic nature of DOS. On the basis of the present studies, we deduce the broadening parameters (σ_1 and σ_2) as listed in Table II for the two materials.

TABLE II. Room temperature broadening parameters extracted from fitting the EA positive wing line shape using Eq. (2).

Material	σ_1 (meV)	σ_2 (meV)
MEH-PPV	56	45
C8-AVPV	42	31

The sum of the two compares well with those reported in the literature for MEH-PPV and other related materials.^{4,31–33} The reported values in the literature are based on the assumption of a single Gaussian or an asymmetric Gaussian as in the case of EA line shape. In our case, σ_1 is certainly due to a defect band adjoining the HOMO level, since the E_F is varied in that range of DOS. The parameter σ_2 could be due to another defect band, or due to intrinsic distribution of conjugation length. In future studies, a better estimate of conjugation length distribution can be done from the negative wing of EA line shape. The sum of the two quantities has been presented earlier as a function of temperature in Fig. 9(b). Therefore, EA and PC for sandwiched diode structures provide a convenient platform to study defect DOS both for fundamental considerations and applications.

IV. CONCLUSIONS

Traditional studies of EA and PC of conjugated polymers lack a careful correlation between the two under well-controlled experimental conditions for otherwise well-characterized materials in sandwich diode configuration. In the literature, typical EA spectra for such structures show a dominant positive peak at the onset whose origin has been controversial. We carry out a careful correlation of PC and EA spectra for two different prototypical materials, viz. MEH-PPV and C8-AVPV, which have different backbone structures. We have shown that the dominant EA peak line shape matches with that of the first derivative of PC spectra at the onset, while the negative peak can get modified due to strong absorption, especially in reflection geometry.

The height of the PC first derivative peak closely follows the temperature dependence of the mobility of the charged carrier indicating the dominance of transport, while the EA peak height is proportional to the density of the states involved in absorption at a particular temperature. With decrease in temperature, EA positive peak becomes narrower and shifts to lower energy showing approximately parabolic dependence on temperature. EA transients at room temperature, monitored sitting at the onset positive peak, are slow and nonexponential. The degree of nonexponentiality, and hence the broadening of the states participating in the transient, decreases with increase in band bending. These observations are consistent with the phenomenological model that the response at the onset is primarily due to photoionization of localized states whose occupancy is controlled by Fermi level and hence its dependence on temperature and bias. This readily explains the common origin of PC and EA line shape and provides a powerful and direct tool to obtain the DOS, which is of significance for transport studies and device applications. The broadening parameter of the DOS for the two materials under study is deduced from the observed line shape.

ACKNOWLEDGMENTS

We are thankful to Girija S. Samal for help in the discussion. We are also thankful to Department of Science and Technology, New Delhi and Samtel group of industries, New Delhi for providing financial support.

APPENDIX A: CORRECTION FACTOR FOR ELECTROABSORPTION IN REFLECTION GEOMETRY

For an organic layer sandwiched between ITO anode and Al cathode, the transmitted light intensity I_t at normal incidence can be written as

$$I_t = I_0(1 - R_1)e^{-\alpha d}(1 - R_2), \quad (\text{A1})$$

where I_0 is the incident light intensity at the ITO/organic layer interface, R_1 and R_2 are the reflection coefficients of front (ITO/organic layer) and back (organic layer/Al) surfaces, respectively, α is the absorption coefficient of the organic material, and d is the thickness of the organic layer. The situation of transmission and reflection for an oblique incidence case is shown in Fig. 14 for visual clarity.

For a simple case where front and back interface have the same reflectivity R and neglecting multiple reflections, Eq. (A1) simplifies to

$$I_t = I_0(1 - R)^2 e^{-\alpha d}. \quad (\text{A2})$$

The change of I_t due to the applied electric field modulation, F , can approximately be expressed as

$$\frac{\partial I_t}{\partial F} = -I_t \left[d \frac{\partial \alpha}{\partial F} + \frac{2}{(1 - R)} \frac{\partial R}{\partial F} \right]. \quad (\text{A3})$$

Using Eqs. (A2) and (A3), one obtains

$$\frac{\Delta I_t}{I_t} = d \Delta \alpha + \frac{2}{1 - R} \Delta R. \quad (\text{A4})$$

For typical organic materials, the Kerr effect is negligibly small and hence the contribution of the change of the reflectance ΔR [second term in Eq. (A4)], due to the applied electric field, to the relative change of the transmission is insignificant. Thus, if T is the transmission coefficient of the organic layer, the EA signal in the case of transmission geometry is given as

$$\frac{\Delta I_t}{I_t} = -\frac{\Delta T}{T} \approx d \Delta \alpha. \quad (\text{A5})$$

For real devices having relatively thick organic layers (typical thickness ~ 100 nm) and the Al cathode acting

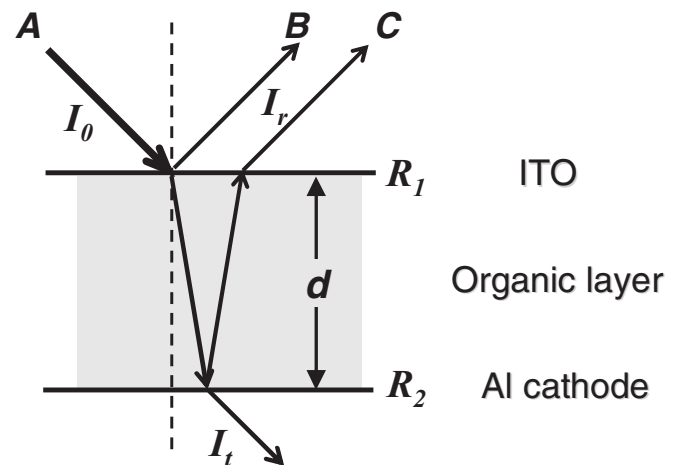


FIG. 14. Situation of transmission and reflection in a thin organic film of thickness d .

as a mirror, the signal-to-noise ratio is too poor to be detected in “transmission” geometry. Hence EA measurement of sandwiched film using the transmission method is not so useful. To monitor the EA response of sandwiched samples, Campbell *et al.*^{18,36} suggested the reflection method in their seminal work.

In the case as shown in Fig. 14, the reflected light intensity I_r at normal incidence can be written as

$$I_r = I_0 R + I_0 R(1 - R)^2 e^{-2\alpha d}. \quad (\text{A6})$$

The change of I_r due to the applied electric field modulation, F , can similarly be expressed as

$$\begin{aligned} \frac{\partial I_r}{\partial F} = & I_0 [1 + (1 - R)^2 e^{-2\alpha d} - 2R(1 - R)e^{-2\alpha d}] \frac{\partial R}{\partial F} \\ & - 2I_0 R(1 - R)^2 e^{-2\alpha d} \frac{\partial \alpha}{\partial F} d. \end{aligned} \quad (\text{A7})$$

Using Eqs. (A6) and (A7), one obtains

$$\begin{aligned} \frac{\Delta I_r}{I_r} = & \left[\frac{1 + (1 - 3R)(1 - R)e^{-2\alpha d}}{1 + (1 - R)^2 e^{-2\alpha d}} \right] \frac{\Delta R}{R} \\ & - \left[\frac{2d(1 - R)^2 e^{-2\alpha d}}{1 + (1 - R)^2 e^{-2\alpha d}} \right] \Delta \alpha, \end{aligned} \quad (\text{A8})$$

where the first term is the contribution from both electroreflectance and Kerr effect (negligible for the case of organic semiconductors, as discussed above). As shown in Fig. 14, the light ray B would get reflected due to field modulation, while the ray C is subjected to electroabsorption. The contribution of the electroreflectance has been found to be insignificant for MEH-PPV thin films.^{13,14} Hence the EA signal in the reflection geometry neglecting electroreflectance is given as

$$\frac{\Delta I_r}{I_r} \approx - \frac{2d(1 - R)^2 e^{-2\alpha d}}{1 + (1 - R)^2 e^{-2\alpha d}} \Delta \alpha. \quad (\text{A9})$$

It is apparent from Eqs. (A5) and (A9) that the qualitative features of the EA spectrum as obtained from transmission and reflection geometry would be similar.

For the case of a thick Al mirror at the back, both I_t and I_r reach the photodetector. If L is the total reflected light intensity ($I_t + I_r$) incident on the photodetector, considering reflections from air/glass and other interfaces, the as-measured EA response ($\Delta L/L$) for sandwiched thin film in reflection geometry is given by

$$\frac{\Delta L}{L} \approx -C(\lambda) \Delta \alpha, \quad \text{where} \quad C(\lambda) = \frac{2d(1 - R)^2 e^{-2\alpha d}}{1 + (1 - R)^2 e^{-2\alpha d}}. \quad (\text{A10})$$

Thus to obtain a correct EA spectrum ($\propto \Delta \alpha$) for sandwiched film in reflection geometry, the as-measured EA signal ($\Delta L/L$) should be corrected using the correction factor $C(\lambda)$ as shown in Eq. (A10). Considering the average reflectivity $R = \sqrt{R_1 R_2}$ of front and back surfaces, both as-measured and corrected EA spectra for a typical ~ 100 -nm MEH-PPV thin film is shown in Fig. 15. It is evident from Fig. 15 that the positive wing line shape of the EA spectrum does not get affected much after correction; however, the strength of the negative wing becomes significant. It suffices to note here that our analysis of the positive wing of the EA spectrum is still valid for the as-measured case.

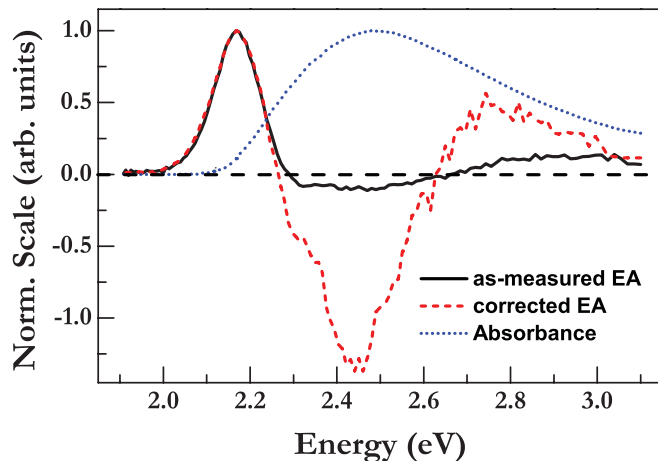


FIG. 15. (Color online) Plot showing the as-measured (black solid line) and corrected (red dash line) EA spectra for a typical ~ 100 nm MEH-PPV sandwiched film. The absorbance (blue dot line) of 100 nm MEH-PPV thin film is also shown for comparison. It is clear here that the positive wing feature of EA response is not sensitive to the correction. However, the negative wing is significantly corrected where the polymer film absorbs well.

APPENDIX B: RELATIONSHIP BETWEEN DENSITY OF STATES AND LINE SHAPE FEATURE

Here we show that the derivative of flux normalized PC spectrum and hence EA spectrum is related to DOS³⁷ by assigning an effective photoionization cross section $\sigma_\phi(h\nu)$ to each state with characteristic threshold energy (E_{th}), as shown in Fig. 16(a). Any energy dependence of σ_ϕ can be ignored for simplicity. For convenience, σ_ϕ can be approximated as a Heaviside step function considering that the PC is due to

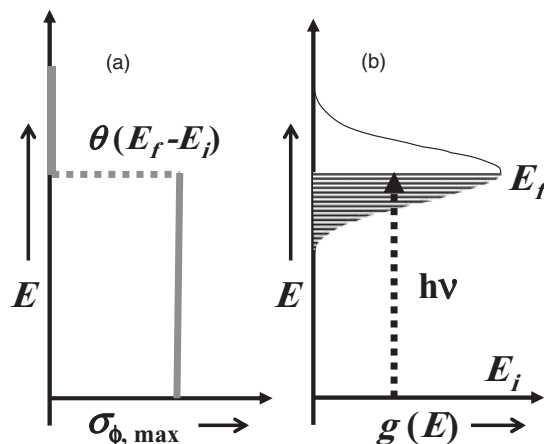


FIG. 16. (a) Assumed simplified shape of photoionization cross section for $E_f - E_i = h\nu$. (b) A pictorial depiction of transitions leading to photoionization due to a transition from initial energy E_i to final energy E_f with a joint DOS shown for E_f only. All energies less than $h\nu$ in E_f will get photoionized.

photoionization of the charge carrier from localized energy states, where $E_{\text{th}} = E_f - E_i$, the difference between final energy E_f and initial energy E_i . Hence all the states below the photon energy $h\nu$ would get effectively photoionized constituting PC. Both E_i and E_f can be distributed, and can be treated as Gaussians as shown in Fig. 16(b). The process can be represented as a transition from E_i to a joint DOS for simplicity. This approach is depicted schematically in Fig. 16.

On the basis of the above argument and assumptions, the PC is given by Eq. (B1),

$$I_{\text{ph}}(h\nu) \propto \int \theta(E_f - E_i - h\nu)g(E_f)dE_f, \quad (\text{B1})$$

where all the terms in the above equation are described above and $g(E_f)$ is the DOS of the final level and $\theta(E)$ is the Heaviside step function. If we take the reference level E_i at zero and set $E_f = \xi$ [see Fig. 16(b)], the derivative of PC is

written as

$$\frac{dI_{\text{ph}}}{d(h\nu)} \propto \int_0^E \delta(\xi - h\nu)g(\xi)d\xi, \quad (\text{B2})$$

$$\frac{dI_{\text{ph}}}{d(h\nu)} \propto g(E_f), \quad (\text{B3})$$

where the δ function results from the differentiation of the step function. Therefore, the derivative of PC action spectra viewed as effective photoionization of localized states is proportional to the DOS. In treatments of photoionization of deep level defects in the context of inorganic semiconductors, the photoionization cross section reduces gently for much higher energies than the threshold.³⁸ Such dependence would also give rise to a gentle zero crossing and a small negative wing in the EA spectra. It may be significant to note that a deep level defect modeled as a quantum defect³⁹ is qualitatively similar to molecular semiconductors, which can be considered as an agglomeration of deep defects with transport energies in the hopping manifold acting as a continuum of states.

*Corresponding author: Department of Physics, Materials Science Programme, Indian Institute of Technology Kanpur, Kanpur-208016, India; ynm@iitk.ac.in

¹*Physics of Organic Semiconductors*, edited by W. Brütting (Wiley-VCH Verlag GmbH & Co. KGaA, Weinheim, 2005).

²*Organic Electronics: Materials, Manufacturing, and Applications*, edited by H. Klauk (Wiley-VCH Verlag GmbH & Co. KGaA, Weinheim, 2006).

³*Ultrafast Dynamics and Laser Action of Organic Semiconductors*, edited by Z. V. Vardeny (Taylor & Francis Group, Boca Raton, 2009).

⁴H. Bässler, *Phys. Status Solidi B* **175**, 15 (1993).

⁵*Primary Photoexcitations in Conjugated Polymers: Molecular Exciton Versus Semiconductor Band Model*, edited by N. S. Sariciftci (World Scientific Publishing Co., Singapore, 1998).

⁶M. G. Harrison, J. Grüner, and G. C. W. Spencer, *Phys. Rev. B* **55**, 7831 (1997).

⁷R. N. Marks, J. J. M. Halls, D. D. C. Bradley, R. H. Friend, and A. B. Holmes, *J. Phys. Condens. Matter* **6**, 1379 (1994).

⁸C. H. Lee, G. Yu, D. Moses, and A. J. Heeger, *Phys. Rev. B* **49**, 2396 (1994).

⁹D. Moses, A. Dogariu, and A. J. Heeger, *Phys. Rev. B* **61**, 9373 (2000).

¹⁰D. Moses, J. Wang, G. Yu, and A. J. Heeger, *Phys. Rev. Lett.* **80**, 2685 (1998).

¹¹T. Stubinger and W. Brütting, *J. Appl. Phys.* **90**, 3632 (2001).

¹²D. Moses, J. Wang, A. J. Heeger, N. Kirova, and S. Brazovskii, *Synth. Met.* **125**, 93 (2002).

¹³T. W. Hagler, K. Pakbaz, and A. J. Heeger, *Phys. Rev. B* **51**, 14199 (1995).

¹⁴M. Liess, S. Jeglinski, Z. V. Vardeny, M. Ozaki, K. Yoshino, Y. Ding, and T. Barton, *Phys. Rev. B* **56**, 15712 (1997).

¹⁵S. J. Martin, D. D. C. Bradley, P. A. Lane, H. Mellor, and P. L. Burn, *Phys. Rev. B* **59**, 15133 (1999).

¹⁶W. P. Su, J. R. Schrieffer, and A. J. Heeger, *Phys. Rev. Lett.* **42**, 1698 (1979).

¹⁷A. Mathy, K. Ueberhofen, R. Schenk, H. Gregorius, R. Garay, K. Müllen, and C. Bubeck, *Phys. Rev. B* **53**, 4367 (1996).

¹⁸I. H. Campbell, T. W. Hagler, D. L. Smith, and J. P. Ferraris, *Phys. Rev. Lett.* **76**, 1900 (1996).

¹⁹C. Giebeler, S. A. Whitelegg, A. J. Campbell, M. Liess, S. J. Martin, P. A. Lane, D. D. C. Bradley, G. Webster, and P. L. Burn, *Appl. Phys. Lett.* **74**, 3714 (1999).

²⁰C. Giebeler, S. A. Whitelegg, D. G. Lidzey, P. A. Lane, and D. D. C. Bradley, *Appl. Phys. Lett.* **75**, 2144 (1999).

²¹J. Yoon, J.-J. Kim, T.-W. Lee, and O.-Ok Park, *Appl. Phys. Lett.* **76**, 2152 (2000).

²²P. A. Lane, J. C. deMello, R. B. Fletcher, and M. Bernius, *Appl. Phys. Lett.* **83**, 3611 (2003).

²³A. K. Biswas, Ashish, A. K. Tripathi, Y. N. Mohapatra, and A. Ajayaghosh, *Macromolecules* **40**, 2657 (2007).

²⁴A. K. Biswas, A. Tripathi, S. Singh, and Y. N. Mohapatra, *Synth. Met.* **155**, 340 (2005).

²⁵A. K. Tripathi, Ashish, and Y. N. Mohapatra, *Org. Electron.* **11**, 1753 (2010).

²⁶K. Pakbaz, C. H. Lee, A. J. Heeger, T. W. Hagler, and D. McBranch, *Synth. Met.* **64**, 295 (1994).

²⁷J. Yu, M. Hayashi, S. H. Lin, K.-K. Liang, J. H. Hsu, W. S. Fann, C.-I. Chao, K.-R. Chuang, and S.-A. Chen, *Synth. Met.* **82**, 159 (1996).

²⁸P. W. M. Blom and M. C. J. M. Vissenberg, *Phys. Rev. Lett.* **80**, 3819 (1998).

²⁹D. Hertel, H. Bässler, U. Scherf, and H. H. Hörhold, *J. Chem. Phys.* **110**, 9214 (1999).

³⁰S. V. Novikov, D. H. Dunlap, V. M. Kenkre, P. E. Parris, and A. V. Vannikov, *Phys. Rev. Lett.* **81**, 4472 (1998).

³¹H. C. F. Martens, P. W. M. Blom, and H. F. M. Schoo, *Phys. Rev. B* **61**, 7489 (2000).

³²C. Tanase, E. J. Meijer, P. W. M. Blom, and D. M. deLeeuw, *Phys. Rev. Lett.* **91**, 216601 (2003).

³³I. N. Hulea, H. B. Brom, A. J. Houtepen, D. Vanmaekelbergh, J. J. Kelly, and E. A. Meulenkaamp, *Phys. Rev. Lett.* **93**, 166601 (2004).

- ³⁴O. Tal, Y. Rosenwaks, Y. Preezant, N. Tessler, C. K. Chan, and A. Kahn, *Phys. Rev. Lett.* **95**, 256405 (2005).
- ³⁵K. Celebi, P. J. Jadhav, K. M. Milaninia, M. Bora, and M. A. Baldo, *Appl. Phys. Lett.* **93**, 083308 (2008).
- ³⁶I. H. Campbell, J. P. Ferraris, T. W. Hagler, M. D. Joswick, I. D. Parker, and D. L. Smith, *Polym. Adv. Technol.* **8**, 417 (1997).
- ³⁷G. S. Samal, Ph.D. thesis, Indian Institute of Technology Kanpur, India, 2007.
- ³⁸B. K. Ridley and M. A. Amato, *J. Phys. C: Solid State Phys.* **14**, 1255 (1981).
- ³⁹B. K. Ridley, *Solid State Electron.* **21**, 1319 (1978).